Available online at www.sciencedirect.com
ScienceDirect
Acta Materialia 56 (2008) 6040–6049
Acta MATERIALIA
www.elsevier.com/locate/actamat

Modeling dislocation storage rates and mean free paths in face-centered cubic crystals

L. Kubin [a,*], B. Devincre [a], T. Hoc [b]

[a] Laboratoire d'Etude des Microstructures, UMR 104 CNRS, CNRS-ONERA, 20 Av. de la Division Leclerc, BP 72, 92322 Chatillon Cedex, France
[b] Laboratoire MSSMat, UMR 8579 CNRS, Ecole Centrale Paris, Grande Voie des Vignes, 92295 Chatenay-Malabry Cedex, France

Received 2 July 2008; accepted 8 August 2008
Available online 1 October 2008

Abstract

The first part of a dislocation-based constitutive formulation for strain hardening in face-centered cubic crystals is presented. This multiscale approach is based on the storage–recovery framework expanded at the scale of slip systems. A parameter-free formulation is established for the critical stress and the storage rate, taking advantage of recent results yielded by dislocation dynamics simulations. The storage rate of dislocations in the presence of forest obstacles is modeled for the first time at the level of dislocation intersections and reactions. The mean free path per slip system is found to be inversely proportional to the critical stress. It also depends on the number of active slip systems, which leads to an orientation dependence of stage II strain hardening in agreement with experimental data. The total storage rate is obtained by including three additional contributions, notably that of the self-interaction, which leads to a model for stage I hardening.

Keywords: Face-centered cubic crystals; Dislocation; Plastic deformation; Strain hardening; Dislocation storage rate

1. Introduction

Predicting on physical bases the mechanical response of crystalline materials is a long-standing objective of dislocation theory. Since early studies on pure single crystals, it is known that the stress–strain curves of face-centered cubic (fcc) crystals exhibit well-defined stages and orientation dependencies (see Refs. [1–3] for reviews). Therefore, modeling these features constitutes a critical test for all models attempting to deal with more complex situations, like the mechanical properties of polycrystals or the response to changes in deformation paths. At present, however, no truly predictive model is able to treat in a seamless manner the complexity of the mechanical response, including the transitions between stages, the number and nature of active slip systems and the corresponding evolutions of the dislocation densities.

We present here the first part of a multiscale approach for the mechanical response of fcc crystals in uniaxial deformation, which incorporates a combination of modeling and simulations (see Ref. [4] for an outline). The modeling part derives from the storage–recovery framework that was developed by Kocks and Mecking [5] for the study of polycrystals and further generalized by Teodosiu and coworkers [6] at the scale of dislocation slip systems. When applied to monotonic deformation, this extended model includes one stored density per slip system, which is assumed to be uniform in space.

For each slip system, the storage–recovery framework includes two major dislocation-based equations: (i) a Taylor-like equation that relates the critical stress on a slip system to the stored densities in all slip systems [7], and (ii) an equation for the net storage rate of dislocations per slip system, which is the sum of a positive storage rate governed by a dislocation mean free path and a negative term accounting for dynamic recovery [5]. The set of equations is closed by a flow rule, which accounts for the strain rate

* Corresponding author. Tel.: +33 1 46 73 4449; fax: +33 1 46 73 4155.
E-mail address: ladislas.kubin@onera.fr (L. Kubin).

1359-6454/$34.00
doi:10.1016/j.actamat.2008.08.012

sensitivity of the material and plays a minor role when the latter is small, as is the case for fcc crystals. Complete solutions for the mechanical response are then obtained by solving this dislocation-based constitutive formulation by a finite element code for crystalline plasticity [8–10]. Many variants of this type of micromechanical model were developed, especially to account for dislocation patterning effects and the response to strain rate changes. This is performed by incorporating additional features like the presence of dislocation walls and the additional modeling of a mobile density or of a density of geometrically necessary dislocations (see e.g. [11–15] for a few representative references). Although this type of modeling represents a progress with respect to previous phenomenological formulations, it always includes a number of free parameters.

To reconstruct the stress–strain curves of bulk fcc crystals without resorting to extensive parameter fitting, advantage is taken of dislocation dynamics (DD) simulations [16,17]. These numerical experiments take advantage of the fact that the complex problems associated with the long- and short-range interactions between dislocation populations can be described to a good approximation within the framework of linear isotropic elasticity [18–20]. DD simulations are used to guide the modeling of the dislocation-based constitutive formulation at the scale of slip systems, as well as to determine the values of the relevant material parameters (see Refs. [4,21,22] for more details).

This paper mainly discusses the components of a constitutive formulation for the plastic deformation of fcc crystals that are based on elastic dislocation mechanisms and interactions. Part 2 is dealing with the generalized form of the Taylor equation, which is further involved in the expression for the storage rate, and emphasizes a proper treatment of line tension effects. In Part 3, the storage rate of dislocations and their mean free path in the presence of a forest density are modeled in terms of dislocation intersections and reactions. These conditions correspond to the linear and athermal stage II of the deformation curves. The total storage rate is obtained in Part 4 by adding three other contributions, especially the one from self-interactions, which leads to a model for strain hardening in stage I. Concluding remarks are presented in Part 5.

2. The critical stress

2.1. The expanded Taylor relation

The Taylor relation implies that the resolved flow stress, τ, is proportional to the square root of a dislocation density ρ, which is assimilated to either the total density [5] or the total density of forest (secondary) obstacles piercing the active slip planes [20,23]:

$$\tau = \alpha\mu b\sqrt{\rho} \tag{1}$$

In this equation μ is the shear modulus, b is the magnitude of the Burgers vector of the dislocations and $\alpha = 0.35 \pm 0.15$ in fcc metals [1,18–20]. To account for the anisotropy of interactions between slip systems, Eq. (1) is expanded in the form [7]:

$$\tau_c^i = \mu b\sqrt{\sum_j a_{ij}\rho^j} \tag{2}$$

where τ_c^i is now the critical stress for the activation of slip system (i), which is determined by dislocation densities in all slip systems (j) including (i) itself. The scalar constant α is replaced by a matrix of coefficients a_{ij} such that $\sqrt{a_{ij}}$ represents the average strength of the interaction between the two slip systems (i) and (j).

2.2. The interaction coefficients

In fcc crystals, the interaction matrix has $12 \times 12 = 144$ coefficients. The number of distinct coefficients is divided by two due to the diagonal symmetry of the matrix ($a_{ij} = a_{ji}$) and the occurrence of four $\langle 1\,1\,1\rangle$ axes with ternary symmetry further divides it by twelve. Hence, there are only six independent coefficients, which are associated with six distinct types of interactions. Three of them account for forest interactions between non-coplanar slip systems, resulting in the formation of junctions or locks, namely the Lomer–Cottrell lock, the Hirth lock and the glissile junction. There are two non-contact interactions for dislocations gliding in parallel slip planes with same or different Burgers vectors, the self-interaction and the coplanar interaction. The last interaction, the collinear interaction, produces annihilations. It occurs between dislocations gliding in two slip planes that are cross-slip planes with respect to each other [17].

The values of the interaction coefficients were recently determined using DD simulations [4,21,22]. They incorporate the strengthening effect of both long- and short-range interactions between dislocations. The interaction coefficients are density-dependent (see Section 2.3) and their values are given in Table 1 for a reference dislocation density of 10^{12} m^{-2}. One may notice from this table that four interaction strengths, $\sqrt{a_{ij}}$, exhibit similar values, those for self, coplanar, glissile and Lomer interactions, while the Hirth type of interaction is slightly weaker and the collinear interaction substantially larger. The high strength of the collinear interaction prevents the activation of collinear slip systems in normal conditions ([17,21], see Section 4.1). As a consequence, the interaction strengths of the active slip systems can be replaced, when necessary and to a reasonably good approximation, by an average interaction strength $\sqrt{a_{ref}} \approx 0.35 = \alpha$.

2.3. Correction for line tension effects

The effective line tension of a bowed out segment includes a logarithmic term [24], which is frequently omitted in the usual forms of the Taylor relation. The effect of this approximation is clearly evidenced in the compilation of experimental data performed by Basinski and Basinski [23] and in further results from DD simulations [20,21].

Table 1
Values of the dimensionless coefficients determining the critical stress and the storage rate in fcc crystals, as implemented in the model (measurement methods and variances are given in the indicated references)

a'_o (self)	a_{copla} (coplanar)		a_{ortho} (Hirth)	a_2 (glissile)	a_3 (Lomer)	a_{coli} (collinear)
0.122 [18]	0.122 (§ 4.2)		0.07 (updated)	0.137 [17]	0.122 [17]	0.625 [17]
p_o	k_o	κ_o	K_{112}	K_{111}	K_{001}	$K_1 = K_{copla}$
0.117	1.08	0.225	10.42	7.29	4.6 (§ 3.4)	180 (§ 4.2)

First two lines: the interaction coefficients values are given for a forest dislocation density of $10^{12} m^{-2}$. The next two lines give from left to right the three coefficients entering the mean free paths for forest interactions [4], the three mean free paths coefficients for symmetrical orientations [4] and the mean free path coefficient for the self and coplanar interactions.

To better describe line tension effects, the critical stress (Eq. (2)) is modified in two steps. First, a logarithmic term accounting for the local line tension is introduced following a procedure that was devised for analyzing the results of DD simulations [21]. This term only applies to the three interaction coefficients related to interactions between junction-forming slip systems. As approximations can be tolerated in the logarithmic term, the curvature radius R^i of segments (i) interacting with a total density ρ_f of junction-forming forest obstacles is taken in the form $R^i \approx \Gamma/b\tau_c^i$, with $\Gamma \approx \mu b^2$ and $\tau_c^i = \mu b\sqrt{\bar{a}_{\mathrm{ref}}\rho_f}$, where the interaction coefficients for forest interactions are replaced by their mean value taken at the reference density of $10^{12}\,\mathrm{m}^{-2}$. The argument of the logarithmic term is then $R^i/b \approx 1/b\sqrt{\bar{a}_{\mathrm{ref}}\rho_f}$ and:

$$a_{ij} = a_{ij,\mathrm{ref}}\left(\frac{\log 1/b\sqrt{\bar{a}_{\mathrm{ref}}\rho_f}}{\log 1/b\sqrt{\bar{a}_{\mathrm{ref}}\rho_{\mathrm{ref}}}}\right)^2 \tag{3}$$

In a second step, the non-local contribution to the line tension, arising from the long-range interactions of a given segment with other segments is taken into account. Foreman [25] showed that, for simple configurations, this contribution introduces a small additive constant to the logarithmic term, which depends on the local environment of the dislocation lines. Large-scale DD simulations performed for forest densities of the order of $\rho_{\mathrm{ref}} = 10^{12}\,\mathrm{m}^{-2}$ indicate that long-range stresses contribute globally to about one-fifth of the critical stress (see, e.g., [26]). Then, the interaction coefficients are eventually written in the form $\sqrt{a_{ij}} = c_f\sqrt{a_{ij}^{\mathrm{ref}}}$, with

$$c_f = 0.2 + 0.8\frac{\log(1/b\sqrt{\bar{a}_{\mathrm{ref}}\rho_f})}{\log(1/b\sqrt{\bar{a}_{\mathrm{ref}}\rho_{\mathrm{ref}}})} \tag{4}$$

Fig. 1 shows a plot of several possible dependencies of this corrective term as a function of the forest density ρ_f. In the range of densities typically spanned along stress–strain curves, the average interaction coefficient can decrease by more than one-half of its initial value, while the relative weight of long-range stresses significantly increases. This fully justifies adopting a more precise treatment of the line tension.

In what follows, the coefficients representing forest interactions incorporate the correction given by Eq. (4). A similar correction should apply in principle to the collinear interaction, which is a particular type of forest reaction. The self-interaction involves a rather complex mixture of mechanisms, and the same probably holds for the coplanar interaction, which seems to behave in the same manner. As there is no obvious way to define the logarithmic correction in terms of the dislocation microstructures, these two coefficients are not corrected (see Section 4.1).

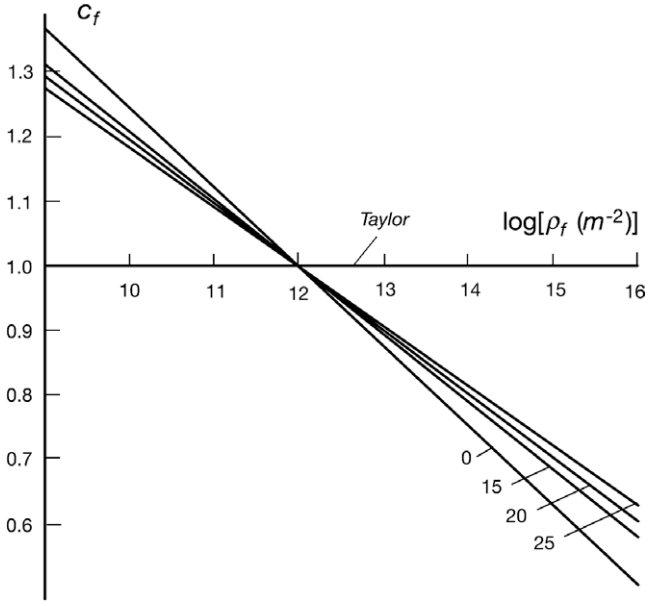

Fig. 1. Various possible dependencies for the coefficient c_f correcting the line tension in the Taylor relation (Eq. (4)) as a function of a density ρ_f of forest dislocations. The drift induced by the logarithmic factor is drawn for four values of the contribution of long-range stresses to the flow stress, 0 (local line tension only), 15, 20 and 25%.

3. Mean free path and storage rate for junction-forming interactions

The formation and destruction of junctions is classically held responsible for strain hardening during stage II [1]. In this part, we estimate the rate at which mobile segments are stored by their interaction with the density already stored in junction-forming (forest) slip systems. For the sake of clarity, the derivation is performed in three steps, which deal, respectively, with the incorporation of junctions in the stored density, the storage rate of an active slip system interacting with an inactive forest and finally the case of

general interest where several active systems mutually interact. Three dimensionless parameters are defined in this part, which are material constants for all fcc crystals. Their values were recently determined by DD simulations [4] and are given in Table 1.

3.1. The treatment of junctions

The junction density constitutes a non-negligible fraction of the stored density (about 30%, see [4,21]), hence special care is taken to account for it. Within the present framework, however, the only dislocation density variables are the densities stored per slip system. As the strengths of the three types of junctions are not very different, both parent segments and junction lines have similar interactions with incoming mobile segments. This allows lumping all junction densities into the densities stored in the active slip systems. This procedure also allows taking into account multijunctions [27,28], i.e. higher order reactions between dislocation lines. The latter occur when a junction formed by a reaction between segments moving in two slip systems further reacts with a segment moving in a third slip system.

In practice, the following procedure is used. A junction between two slip systems (i) and (j) can be formed in two different manners. It can be formed by mobile dislocations of system (i) that react with the stored forest density (j) or vice versa. We make a distinction between these two types of junctions by using the notation ($i \to j$) or ($j \to i$), where the first index is that of the moving dislocations. Then, as illustrated by Fig. 2, dislocations of type ($i \to j$) or ($j \to i$) are converted into stored densities in slip systems (i) and (j), respectively. Although one can imagine different manners of distributing junction densities into the stored densities, the present one is most reasonable. Indeed, it does not attribute large junction densities to weakly active slip systems having relatively small stored densities. Using this procedure entails, however, distinguishing between reacting and non-reacting junctions. As shown in Fig. 2, a junction line of type ($i \to j$), which is lumped into slip system (i), cannot constitute a forest obstacle for further incoming segments in system (j). It can nevertheless react with all other forest slip systems of (i).

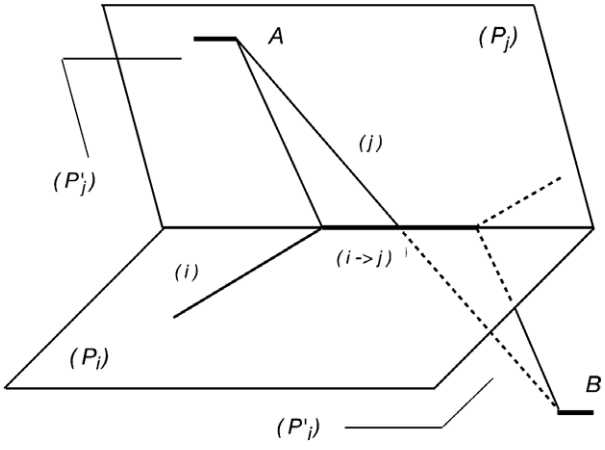

Fig. 2. This figure is drawn in the slip plane (P_j) of a stored segment (j) pinned by junctions at A and B. In a plane (P_i), an incoming dislocation (i) has formed a junction of type ($i \to j$) along the intersection line of the two slip planes. By convention, the junction line is attributed to slip system (i) and interacts with (i) dislocations gliding in planes (P'_i) via the self-interaction. This junction is, however, not a forest obstacle for dislocations (j) moving in slip planes (P'_j).

3.2. Storage rate induced by non-active forest slip systems

In what follows, the subscript (o) denotes variables specific to this section, which will be further rediscussed. In a first step, we consider a slip system (i) interacting with an inactive forest consisting of slip systems (j) $\neq$ (i), in density ρ_o^j. This forest is made up of segments of average length $\bar{\ell}_o^j$. According to the rule defined above for redistributing junctions into slip systems, all the junctions formed during the motion of dislocations (i) are attributed to slip system (i). Then, each segment stored in (i), of average length $\bar{\ell}_o^i$, contains two parent segments and one junction (Fig. 2). In a volume V of crystal, during a shear increment $\mathrm{d}\gamma^i$ on system (i), the swept area is $\mathrm{d}A^i = \mathrm{d}\gamma^i V/b$. The number of intersections occurring in the swept area between dislocations (i) and forest segments (j) is denoted $\mathrm{d}N^{i\to j}$. In the direction perpendicular to the slip planes of (i), the forest segments have a projected height $\phi\bar{\ell}_o^j$ (Fig. 2), where ϕ is a geometrical factor taking into account their average inclination with respect to the primary slip planes ($\phi \approx 0.6$, see Appendix A). The total length stored in a volume $\mathrm{d}A^i\phi\bar{\ell}_o^j$ is $\mathrm{d}N^{i\to j}\bar{\ell}_o^j$ and the density of forest trees in this volume is $\rho_o^j = \mathrm{d}N^{i\to j}/\phi\mathrm{d}A^i$. Thus, the number of intersections of type ($i \to j$) is:

$$\mathrm{d}N^{i\to j} = \phi\rho_o^j \mathrm{d}A^i = \phi\rho_o^j \mathrm{d}\gamma^i V/b \tag{5}$$

Repulsive intersections, as well as weakly attractive junctions cannot form junctions, so that only a fraction f_o of the total number of intersections is actually forming stable reaction products under stress. This fraction is taken proportional to the strength of the interaction between slip systems (i) and (j), $\sqrt{a_{ij}}$, so that the number of junctions formed, $\mathrm{d}N_{jct}^{i\to j}$, is written $\mathrm{d}N_{jct}^{i\to j} = f_o\sqrt{a_{ij}}\mathrm{d}N^{i\to j}$. The total number of junctions formed with all forest systems (j) during the shear increment $\mathrm{d}\gamma^i$ is then written $\mathrm{d}N_{jct}^{i\to}$. It is obtained by replacing the number of intersections $\mathrm{d}N^{i\to j}$ by its value, as given by Eq. (5), and performing a summation over all forest slip systems:

$$\mathrm{d}N_{jct}^{i\to} = p_o \frac{V}{b}\left(\sum_{j\in f^i}\sqrt{a_{ij}}\rho_o^j\right)\mathrm{d}\gamma^i \tag{6}$$

In this expression, $p_o = f_o\phi$ is a dimensionless constant and the index f^i refers to all the forest slip systems seen by dislocations (i).

The formation of each junction stores a length $\bar{\ell}_o^i$ in system (i) and increments the density stored by $\bar{\ell}_o^i/V$. The total density $\mathrm{d}\rho_o^i$ stored in system (i) during a shear strain increment $\mathrm{d}\gamma^i$ is then given by $\bar{\ell}_o^i dN_{jct}^{i\to}/V$. Combining this expression with Eq. (6), we have:

$$\frac{\mathrm{d}\rho_o^i}{\mathrm{d}\gamma^i} = \frac{p_o \bar{\ell}_o^i}{b}\left(\sum_{j\in f^i}\sqrt{a_{ij}}\rho_o^j\right) \tag{7}$$

The average length $\bar{\ell}_o^i$ of the stored segments (i), which appears in Eq. (7), can be estimated in a straightforward manner. As is known from dislocation theory, $\bar{\ell}_o^i$ is inversely proportional to the critical stress on system (i). Hence, one can write $\bar{\ell}^i = k_o \mu b/\tau_c^i$, where k_o is a second dimensionless constant. Making use of Eq. (2), we have:

$$\bar{\ell}_o^i = \frac{k_o}{\sqrt{\sum_j a_{ij}\rho_o^j}} \tag{8}$$

It follows from the definition of the critical stress that the summation in the denominator has to be carried out on all slip systems.

The density of junctions in the active slip system can now be derived. From the ratio of junction lengths $\bar{\ell}_{jct}^i$ to the corresponding average segment lengths $\bar{\ell}_o^i$, or, equivalently, of the related densities, one can define a third dimensionless constant:

$$\kappa_o = \frac{\rho_{jct}^i}{\rho_o^i} = \frac{\bar{\ell}_{jct}^i}{\bar{\ell}_o^i} \tag{9}$$

DD simulations show that κ_o is a constant to a good approximation [4].

3.3. Storage rate induced by active forest slip systems

In this last step, we relax the assumption that forest slip systems are inactive, which entails modifications in the densities and average lengths of active slip systems. These quantities are denoted like in the previous step, except that the index (o) is removed. During a shear strain increment $\mathrm{d}\gamma^i$, the forest slip systems of (i) may produce a shear strain increment $\mathrm{d}\gamma^j$. They form junctions of type ($j \to i$) with the density stored in (i), which are transferred from system (i) to its forest systems. The total junction density of this type is written:

$$\rho_{jct}^{\to i} = \sum_{j\in f^i}\rho_{jct}^{j\to i} \tag{10}$$

and the density ρ^i is given by:

$$\rho^i = \rho_o^i - \rho_{jct}^{\to i} \tag{11}$$

The average length of segments (i), $\bar{\ell}_o^i$, is also reduced and becomes $\bar{\ell}^i$, while the corresponding densities are reduced in the same proportion. One then has:

$$\frac{\bar{\ell}^i}{\rho^i} = \frac{\bar{\ell}_o^i}{\rho_o^i} \tag{12}$$

This ratio is not a constant because its evolution with strain depends on the activity of the forest slip systems. Eliminating ℓ_o^i and ρ_o^i from Eq. (12) with the help of Eqs. (8) and (11), one easily obtains:

$$\bar{\ell}^i = \frac{k_o}{\sqrt{\sum_j a_{ij}(\rho^j + \rho_{jct}^{\to j})}}\left(\frac{\rho^i}{\rho^i + \rho_{jct}^{\to i}}\right) \tag{13}$$

The reasoning used to derive the storage rate given by Eq. (7) is now applied to the incremental stored density $d\rho^i$. The net result amounts to simply replacing the average length $\bar{\ell}_o^i$ by $\bar{\ell}^i$ and the forest densities ρ_o^j by ρ^j. This accounts, respectively, for the transfer of junction densities from slip system (i) to its forest systems and vice versa. In addition, dislocations (i) do not see the junctions of type ($j \to i$) as forest obstacles (cf. Fig. 2). This density of non-reacting junctions is, therefore, removed from the density ρ^j, which becomes $\rho^j - \rho_{jct}^{j\to i}$. Eq. (7) is then rewritten as:

$$\frac{\mathrm{d}\rho^i}{\mathrm{d}\gamma^i} = \frac{p_o \bar{\ell}^i}{b}\left(\sum\nolimits_{j\in f^i}\sqrt{a_{ij}}\rho^j\right)\left(1 - \frac{\sum_{j\in f^i}\sqrt{a_{ij}}\rho_{jct}^{j\to i}}{\sum_{j\in f^i}\sqrt{a_{ij}}\rho^j}\right) \tag{14}$$

As the last term at the right-hand side of this equation is a corrective term, it can be simplified by replacing the interaction coefficients in the numerator and the denominator by their average value (cf. Section 2.3). One eventually obtains:

$$\frac{\mathrm{d}\rho^i}{\mathrm{d}\gamma^i} = \frac{1}{b}\frac{p_o k_o}{\sqrt{\sum_j a_{ij}(\rho^i + \rho_{jct}^{\to j})}}\left(\frac{\rho^i}{\rho^i + \rho_{jct}^{\to i}}\right)\left(\sum_{j\in f^i}\sqrt{a_{ij}}\rho^j\right)\left(1 - \frac{\rho_{jct}^{\to i}}{\rho_f^i}\right) \tag{15}$$

where the average length $\bar{\ell}^i$ is replaced by its value given by Eq. (13). One can note at this step that the storage rate has the dimension of the square root of a dislocation density. This point will be further developed in Section 4.3.

To obtain the final form of this storage rate, one has to estimate junction densities of the form $\rho_{jct}^{\to j}$ or $\rho_{jct}^{\to i}$, which are involved in Eqs. (13) and (15). This calculation is performed in Appendix B, by deriving an evolutionary law for the storage rate of these densities. One obtains (Eqs. (B.5) and (B.6)):

$$\mathrm{d}\rho_{jct}^{\to i} = \kappa_o \frac{p_o k_o}{b}\frac{\rho^i \sum_{j\in f^i}\sqrt{a_{ij}}\mathrm{d}\gamma^j}{\sqrt{\sum_j a_{ij}(\rho^j + \rho_{jct}^{\to j})}}\left(1 - \frac{\rho_{jct}^{\to i}}{(n-1)\rho^i}\right) \tag{16}$$

In this equation, the constant κ_o is defined by Eq. (8) and n is the number of active slip systems, so that $(n-1)$ is the number of forest systems seen by system (i). Once it is inserted into the whole constitutive formulation, the set of coupled Eqs. (15) and (16) allows estimating the storage rate due to forest interactions.

3.4. A textbook case: symmetrical multiple slip

The properties of the mean free path associated with forest interactions become more transparent in the case of deformation along high symmetry orientations, that is, in symmetrical multiple slip conditions. To keep this example simple, the interaction coefficients are replaced by their average value and the line tension correction is omitted.

The slip systems indexes are now removed and the density and incremental shear strain per slip system are denoted ρ and $\mathrm{d}\gamma$, respectively. The total stored density is

$\rho_t = n\rho$ and the forest density associated with each slip system is $\rho_f = (n-1)\rho$. In each slip system, the line density lost by junction transfer to other slip systems, $\rho_{jct}^{\rightarrow i}$, is identical to the density of junctions transferred from other slip systems, $\rho_{jct}^{i\rightarrow}$, and $\rho_{jct}^{\rightarrow i} = \rho_{jct}^{i\rightarrow} = \rho_{jct}$. From Eqs. (9) and (11), one has:

$$\kappa_o = \frac{\rho_{jct}}{\rho_o} = \frac{\rho_{jct}}{\rho + \rho_{jct}} \tag{17}$$

from which one draws:

$$\rho_{jct} = \rho \frac{\kappa_o}{1-\kappa_o} = \kappa\rho \tag{18}$$

This expression defines a new constant, $\kappa = \kappa_o/(1-\kappa_o)$, which is specific to symmetrical deformation conditions.

Using these new notations, the evolutionary Eq. (15) yields the storage rate in each slip system or, equivalently, the total storage rate:

$$\frac{\mathrm{d}\rho}{\mathrm{d}\gamma} = \frac{\mathrm{d}\rho_t}{\mathrm{d}\gamma_t} = \frac{1}{bL_f} = \frac{p_o k_o}{b} \frac{\rho_f}{\sqrt{\rho_t}(1+\kappa)^{3/2}} \left(1 - \frac{\kappa}{n-1}\right) \tag{19}$$

where L_f is the mean free path associated with forest interactions. The density terms at the right-hand side reduce to $(n-1)\sqrt{\rho_t}/n$. Rearranging the terms to introduce the critical stress, one has:

$$\frac{1}{L_f} = \frac{p_o k_o}{(1+\kappa)^{3/2}} \frac{\tau_c}{\mu b\sqrt{\bar{a}}} \left(\frac{n-1-\kappa}{n}\right) \tag{20}$$

From this expression, one can see that the mean free path associated with forest interactions exhibits two important properties. First, it is inversely proportional to the critical stress or to the square root of the total density. The second property is a dependence of the storage rate on the number n of active slip systems, through its total forest density, which induces an orientation dependence of strain hardening in stage II. This feature was never consistently modeled, although it is clearly visible in experimental stress strain curves [1,3]. Lumping all constant coefficients into a dimensionless and orientation-dependent coefficient K_{hkl}, the mean path L_f can eventually be set in the simple forms:

$$L_f = K_{hkl} \frac{\mu b}{\tau_c} = \frac{K_{hkl}}{\sqrt{\bar{a}\rho_t}} \tag{21}$$

The coefficient K_{hkl} depends on the average interaction strength and on the set of constants p_o, k_o and κ_o (or κ). The values of these last constants can hardly be calculated but are conveniently computed using DD simulations ([4], see Table 1). This allows cross-checking the value of the coefficient K_{hkl}, which can also be estimated from Eqs. (20) and (21), and verifying that the proposed model reproduces well the output of DD simulations.

In symmetrical conditions and in stage II, the strain hardening matrix reduces to a scalar term $\theta_{II} = \mathrm{d}\tau_c/\mathrm{d}\gamma_t$. This term can be obtained as the product of the derivative of the critical stress (Eq. (2)) with respect to the total density, $\mathrm{d}\tau_c/\mathrm{d}\rho_t$, by the total storage rate (Eq. (20)). Omitting the logarithmic dependence of the interaction coefficients, one easily obtains a constant work hardening rate for each orientation of the loading axis:

$$\frac{\theta_{II}}{\mu} = \frac{\bar{a}}{2K_{hkl}} \propto \frac{n-1-\kappa}{n} \tag{22}$$

The work hardening rate in stage II was computed from a form similar to Eq. (22), obtained by taking into account a logarithmic dependence of the coefficient $\bar{a}$ through Eq. (3). The stress–strain curves are integrated in a strain domain that is representative of stage II behavior. The results are shown in Fig. 3 for copper crystals ($\mu = 42$ GPa, $b = 0.256$ nm). The linear work hardening slopes are in close agreement with commonly measured values, especially those given in the detailed study by Takeuchi [29]. For instance, the work hardening rate is $\theta_{II} = \mu/290$ for the $[\bar{1}12]$ orientation and is about two times this value for the [001] orientation (2.5 times upon making the correction discussed in Section 4.1). In the same way, the maximum hardening slopes at small strains are close to those measured by Takeuchi (see Fig. 9 of Ref. [29]). Finally, the rather simple form of the strain hardening rate given by Eq. (22) allows justifying the incorporation of junction lines into the present model, and the complications it entails, through its non-negligible impact on strain hardening (cf. Appendix C).

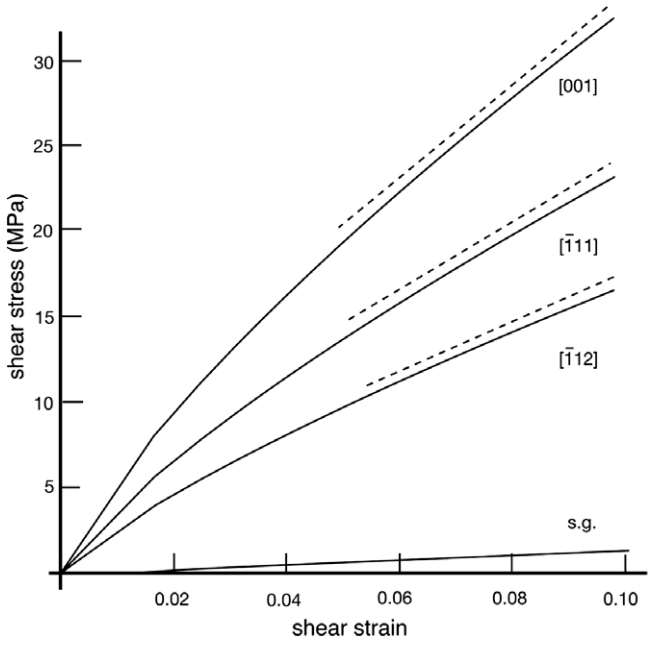

Fig. 3. Computed shear stress–shear strain curves of copper crystals for three symmetrical orientations showing linear stage II slopes (dashed lines). The slight curvatures are due to the drift of the interaction coefficients induced by line tension effects (Section 2.3). The curve *s.g.* is drawn for single glide in the presence of a constant forest density of 10^9 m^{-2} (Section 4.2).

4. Other storage rates

The total storage rate includes contributions from three additional interactions. The first one arises from collinear slip, i.e., the simultaneous activation of a slip system and its cross-slip system. Collinear annihilations can be modeled as a particular type of forest interaction resulting in the formation of junctions with null Burgers vector. For the present purpose, however, this contribution can be accounted for in a simple manner. A model for the self-interaction and its application to single slip in stage I was proposed in [30] and we present here an updated version, which is partly based on recent results from DD simulations [22]. The last contribution to the storage rate is due to coplanar duplex slip. These three contributions arise from the occurrence of either collinear segments or small collinear superjogs and they involve rather complex dislocation interactions.

4.1. Collinear double slip

As was shown in previous publications [17,21], unconstrained double collinear glide is unstable due to the high strength of the collinear interaction and results in the selection of one of the two slip systems at the expense of the other. In uniaxial deformation, this situation is met for two loading axes, $[\bar{1}11]$ and [001], for which both the slip and cross-slip systems have the maximum Schmid factor. The selection rule being verified for the $[\bar{1}11]$ orientation [31], there is no point in introducing a storage rate due to collinear slip in that case. The model then predicts the occurrence of three active slip systems, whereas six are potentially active.

The situation is more confused for orientations in the immediate vicinity of [001]. Slip traces corresponding to all collinear slip systems are observed but, in general, only one set of two collinear slip systems is found to be active in a given area of the specimen's surface [32]. In parallel, strain hardening substantially increases within two to four degrees from the exact orientation [33]. DD simulations carried out up to strains of the order of 1% [22] reveal in this case the occurrence of a mechanism that is specific to the [001] orientation. In substance, collinear segments are dragged by primary segments, which enforces the activation of collinear dislocation sources and of collinear slip. This mechanism not being incorporated into the present model, DD simulations show that the predicted storage rate is too small by a factor of 1.35 [4]. This difference is due to reactions between the collinear density and its cross-slip and forest systems. To account for it in the case of forest interactions in the [001] orientation, the storage rate yielded by the model is simply multiplied by the missing factor.

4.2. Storage rate induced by self and coplanar interactions

The influence of the self-interaction manifests itself clearly during the low strain hardening stage, also called stage I or easy glide stage, that is observed when a single slip system is active. The main two characteristic features of the microstructures formed in this stage are: (1) the occurrence of dipolar or multipolar bundles of dislocation loops made up of elongated primary edge segments and short collinear jogs, and (2) the striking absence of any significant screw density. As discussed in [2,22], this microstructure is formed through a complex sequence of events. The collinear jogs are produced by the mutual annihilation of screw dislocations by cross-slip, which is mostly stress-driven under the low applied stress. This process leads to the formation of a small density of very short edge segments in the cross-slip planes of the primary slip system. After rather complex interactions, these superjogs are stored in the elongated dipolar loops. In a critical review of models for stage I, Nabarro [2] lists evidences according to which stage I hardening is not due to dipole formation and destruction but arises from the stress-driven annihilation of screw segments by cross-slip and the subsequent formation of collinear superjogs. This approach is revisited below.

Basinski [23] showed that the Taylor relation can be extrapolated down to the low-stress stage I, which indicates the presence of forest hardening. The latter is attributed to forest dislocations, of which the density is experimentally found to be a constant fraction, typically 10%, of the primary density [1,22]. These forest dislocations essentially arise from the continuous production of a collinear superjog density of about $0.1\rho^p$, and strongly interact with the primary dislocations. The contribution of this density to forest hardening is then written in the form $a'_o\rho^p$, where the coefficient a'_o accounts for both the constant ratio of collinear to primary density and the strength of the interaction between primary mobile segments and superjogs. Due to the small size of the latter, this interaction cannot be treated like a typical forest interaction between segments of length $\rho^{-1/2}$. The self-interaction coefficient a'_o should, nevertheless, have a value typical of forest interactions since the Taylor relation is experimentally verified. This was confirmed by DD simulations incorporating a density $0.1\rho^p$ of collinear superjogs [22], which yielded $a'_o \approx a_3 = 0.122$, where a_3 is the interaction coefficient associated with the interaction between primary and conjugate slip.

By analogy with symmetrical multiple slip (Eq. (21)), the storage rate is written in the form:

$$\frac{\mathrm{d}\rho^p}{d\gamma^p} = \frac{1}{bL_I} = \frac{\sqrt{a'_o\rho^p}}{bK_I} \tag{23}$$

The plastic strain γ^p is carried out by segments of all characters, and L_I and K_I denote respectively the mean free path for self-interactions and the related mean free path constant. Because Stage I involves a multiplicity of interaction mechanisms and a very long mean free path, it seems difficult to fully model it with the aid of DD simulations. In what follows, we estimate a plausible value for the constant K_I.

We assume that the primary density stored in the form of edge dipolar or multipolar bundles represents the totality of the edge density that was produced by multiplication mechanisms. In parallel, the whole screw density that was produced was annihilated, leading to the storage of a collinear density of about $0.1\rho^p$. Dislocation segments are elongated in the screw direction, due to the smaller line energy in the screw orientation. The aspect ratio of half-loops, which we assimilate to the ratio of screw to edge densities, is about 1.7 in copper, according to refined calculations in anisotropic elasticity [34,35], with, however, a significant uncertainty. Thus, a screw density of about $1.7\rho^p$ has resulted in the storage of a collinear density of $0.1\rho^p$, that is, 17 times less. Forest interactions, as modeled in Part 3, involve storage events but no annihilations. Thus, in terms of storage rate, the self-interaction is less efficient than a forest mechanism and, with $K_{112} = 10.4$ (cf. Table 1), one should have $K_I \approx 17K_{112} \approx 180$. Although this value is implemented in the present model, it must be noted that it involves some uncertainty. For a stress of 1 MPa, this corresponds to a mean free path value $L_I \approx 1.8$ mm, which is large in comparison to the typical slip line lengths of 600 μm measured in stage I [4]. As discussed in Part 5 this difference is inherent to the continuous description of the mean free path.

The strain hardening coefficient is derived like in Section 3.4. As the effect of the initial forest density becomes negligible soon after the yield stress, Eq. (23) is combined with the derivative of the critical stress $\tau_c^p \approx \mu b\sqrt{a'_o\rho^p}$ with respect to the primary density. In simplified terms, the strain hardening rate takes a form similar to that of Eq. (21), $\theta_I \approx a'_o/2K_I$. Fig. 3 shows a resolved stress vs. strain curve for single glide, calculated for a constant forest density of $10^9\,\mathrm{m}^{-2}$ and with $a'_o = 0.122$ and $K_\mathrm{I} = 180$. The strain hardening rate is $\theta_I = \mu/3100$, in agreement with experimental values [3].

Very little is known about the interaction between coplanar slip systems, as the corresponding microstructures have never been investigated to the knowledge of the present authors. Double coplanar slip is often observed along the lower portion of the $[011] - [\bar{1}11]$ zone axis and close to the [011] orientation [29]. The corresponding stress–strain curves exhibit an initial strain hardening stage quite similar to that of stage I, as was first noted by Jackson [36]. This suggests that the coplanar and self-interactions have in common the formation of a small collinear density via screw dislocation cross-slip and can be treated in a similar manner. For this reason, we take $a_{copla} = a'_o$ for the interaction coefficient and $K_{copla} = K_I$ for the mean free path constant.

4.3. Total storage rate

The total storage rate, excluding the negative term arising from dynamic recovery, is obtained by summing the individual storage rates or the inverses of the related mean free paths:

$$\frac{\mathrm{d}\rho^i}{\mathrm{d}\gamma^i} = \frac{1}{b}\left(\frac{1}{L_f} + \frac{\sqrt{a'_o\rho^i}}{K_I} + \frac{\sum\limits_{j\in copla(i)}\sqrt{a_{copla}\rho^j}}{K_{copla}}\right) \tag{24}$$

The first term at the right-hand side describes the contribution from the three junction-forming interactions. The second term accounts for the self-interaction and the third term accounts for coplanar interactions. This last term includes a summation since a slip system has two possible coplanar slip systems in the fcc structure.

5. Concluding remarks

The present work presents the major part of a dislocation-based constitutive formulation for strain hardening in fcc crystals, which is based on the storage–recovery framework expanded at the scale of slip systems. A substantial effort is devoted to establish a parameter-free model, taking advantage of a wealth of information recently yielded by DD simulations. As a result, a set of dimensionless coefficients valid for all fcc crystals is proposed, which allows bypassing parameter-fitting procedures.

It is shown that refining the critical stress to include a logarithmic term removes a significant source of numerical inaccuracy. The storage rate of dislocations in the presence of forest obstacles, or alternatively the mean free path of dislocations, is modeled for the first time at the level of average dislocation intersection mechanisms. In particular, care is taken to account for the presence of a junction density in the microstructure. The storage rate is found proportional to the critical stress and it exhibits a dependence on orientation that is directly related to the number of active forest slip systems interacting with each active slip system. This allows explaining the orientation dependence of strain hardening in stage II, in agreement with experimental data. The total storage rate is obtained by including three additional contributions from non-forest interactions. The most important one is the self-interaction, for which an additional model that leads to stage I hardening is proposed. As the formulation presented here is mostly dealing with elastic interactions, it is potentially adaptable to a variety of crystal structures.

The difference noted in Section 4.2 between the continuum mean free path L_I and the length of slip traces during stage I arises from the quite general fact that although these two lengths are related, they are not identical. In the recent years, investigations of dislocation avalanches and the intermittent nature of dislocation glide in crystals ([37], see the review [38]) have brought a new insight into the statistical properties of collective slip events produced by dislocation strain bursts. A recent study by DD simulations [4], showed, however, that this intermittent behavior and the present continuum model can be made fully compatible through a coarse-graining procedure. A consequence of interest is that the mean free path values defined in the continuum are virtual

because they do not describe the real strain burst behavior. After coarse-graining, the intermittent storage rate of avalanches is replaced by a storage rate that is necessarily smaller since it evolves in a continuous manner. It follows that continuum mean free paths are larger than characteristic avalanche dimensions, that is, typically, slip line lengths. This explains the origin of the above-mentioned difference.

At this step, one may note that elastic dislocation processes are treated without accounting directly or indirectly for dislocation patterning phenomena. This can be justified from the fact that the Taylor relation is rather insensitive to the spatial arrangement of the dislocation microstructure [20,23]. Since the two basic constitutive relations discussed in the present work incorporate this relation in the form of a critical stress, there is no need to introduce any additional feature accounting for dislocation patterning. This holds true at least for monotonic uniaxial loading. In such conditions, the use of a single dislocation density variable per slip system seems justified. In forthcoming papers, the present model will be completed and solved using a crystal plasticity code in order to predict the mechanical response of fcc crystals and compare it to experimental data. This will allow discussing its limitations and possible extensions in more depth.

Appendix A. The geometrical factor ϕ

We consider two slip systems with slip planes (111) and $(\bar{1}11)$, which intersect each other along the screw direction $[0\bar{1}1]$. One can check easily that the random unit direction of dislocation lines in the $(\bar{1}11)$ plane can be parametrized in the form $[2t, t-\sqrt{1-t^2}, t+\sqrt{1-t^2}]/\sqrt{4t^2+1}]$, where t ranges from 0 for the screw direction to 1 for the edge direction [211]. The angle θ between this random direction and the [111] normal is given by $\cos\theta = 4t/\sqrt{3(4t^2+2)}$. Assuming a uniform distribution of dislocation characters, the geometrical constant ϕ is the average value of $\cos\theta$ between $t=0$ and $t=1$. By taking $u=4t^2$ as variable, the integration step is carried out in a straightforward manner, leading to: $\phi = (\sqrt{6}-\sqrt{2})/\sqrt{3} \approx 0.6$.

Appendix B. Evolutionary law for junction densities

An evolutionary law for the total junction density $\rho_{jct}^{\rightarrow i}$, which is transferred from slip system (i) to its forest density, is established by retracing the steps made in the text to derive the storage rate. Eq. (5) was obtained by considering that slip system (i) is active, whereas its forest systems are inactive. This equation is rewritten for the opposite situation where slip system (i) is inactive, whereas its forest slip systems are active. This yields:

$$\mathrm{d}N_{jct}^{\rightarrow i} = p_o\left(\sum_{j\in f^i}\rho_o^i\sqrt{a_{ij}}d\gamma^i\right)V/b \tag{B.1}$$

According to Eq. (9), all junctions involving system (i) have the same length $\bar{\ell}_{jct}^i = \kappa_o\bar{\ell}_o^i$, so that the incremental junction density transferred to the forest slip systems is $\kappa_o\bar{\ell}_o^i\mathrm{d}N_{jct}^{\rightarrow i}$. One then obtains an expression analogous to Eq. (7):

$$\mathrm{d}\rho_{jct}^{\rightarrow i} = \kappa_o\frac{p_o\bar{\ell}_o^i}{b}\left(\sum_{j\in f^i}\rho_o^i\sqrt{a_{ij}}d\gamma^j\right) \tag{B.2}$$

The condition that the density ρ_o^i is immobile is now relaxed by replacing ρ_o^i by ρ^i. The average length of junctions $\bar{\ell}_{jct}^i = \kappa_o\bar{\ell}_o^i$ is not modified since it is not affected by their redistribution among slip systems. In addition, mobile dislocations (j) do not see the junctions of type ($i\rightarrow j$) as forest obstacles (Fig. 2) and the density of non-reacting junctions $\rho_{jct}^{i\rightarrow j}$ has to be removed from the density ρ^i. One then obtains:

$$\mathrm{d}\rho_{jct}^{\rightarrow i} = \kappa_o\frac{p_o\bar{\ell}_o^i}{b}\left(\sum_{j\in f^i}\sqrt{a_{ij}}(\rho^i-\rho_{jct}^{i\rightarrow j})d\gamma^j\right) \tag{B.3}$$

The summation applies to all terms containing an index (j), the density ρ^i being incorporated into it for convenience. After some manipulation, one obtains an expression analogous to Eq. (18):

$$\mathrm{d}\rho_{jct}^{\rightarrow i} = \kappa_o\frac{p_o\bar{\ell}_o^i\rho^i}{b}\left(\sum_{j\in f^i}\sqrt{a_{ij}}d\gamma^j\right)\left(1-\frac{\sum_{j\in f^i}\sqrt{a_{ij}}\rho_{jct}^{i\rightarrow j}\mathrm{d}\gamma^j}{\rho^i\sum_{j\in f^i}\sqrt{a_{ij}}\mathrm{d}\gamma^j}\right) \tag{B.4}$$

The elementary junction densities $\rho_{jct}^{i\rightarrow j}$ cannot be estimated within the present framework. We then assume by default that they are all identical. If there are n active slip systems, the summation on the junction densities yields $\rho_{jct}^{i\rightarrow j} = \rho_{jct}^{i\rightarrow}/(n-1)$. This leads to an exact result in two important extreme cases. The first one is symmetrical multislip conditions, where densities are identical in all active slip systems. The second one is the highly dissymmetrical transition between stage I and stage II, during which the primary slip system interacts with a single active forest system. In that case, $n=2$ and $\rho_{jct}^{i\rightarrow j} = \rho_{jct}^{i\rightarrow}$. Within this approximation, the general deformation conditions are treated by interpolation between these two extreme cases. The last term at the right-hand side of Eq. (B.4) reduces to $\rho_{jct}^{i\rightarrow}/(n-1)\rho^i$ and the final result is written:

$$d\rho_{jct}^{\rightarrow i} = \kappa_o\frac{p_o\bar{\ell}_o^i\rho^i}{b}\left(\sum_{j\in f^i}\sqrt{a_{ij}}d\gamma^j\right)\left(1-\frac{\rho_{jct}^i}{(n-1)\rho^i}\right) \tag{B.5}$$

where the average length $\bar{\ell}_o^i$ can be deduced from Eqs. (8) and (11):

$$\bar{\ell}_o^i = \frac{k_o}{\sqrt{\sum_j a_{ij}(\rho^i+\rho_{jct}^{\rightarrow i})}} \tag{B.6}$$

The combination of Eqs. (B.5) and (B.6) leads to Eq. (16) of the text.

Appendix C. The impact of junction densities on strain-hardening

The results obtained in Section 4.3 allow answering in simple terms the following question: what is the effect of junctions on strain hardening? The effect of usual (binary) junctions is directly obtained from Eq. (22) by setting the junction length to zero, i.e., by taking $\kappa = 0$. The orientation factor $(n-1-\kappa)/n$ then becomes $(n-1)/n$. With $\kappa = 0.3$ (Table 1), the strain hardening rate increases by 30% for the $[\bar{1}12]$ orientation and the ratio of strain hardening rates between [001] and $[\bar{1}12]$ decreases by 28%. These differences are substantial.

We now consider the effect of neglecting multijunctions, that is, reactions of mobile dislocations with non-coplanar binary junctions [28], which occur for the [001] and $[\bar{1}11]$ orientations. In this case, the formation of binary junctions is accounted for but their further reaction with dislocations on intersecting slip systems is forbidden. In Eq. (19), the last term at the right-hand side accounts for the non-interacting junction density, as defined in Fig. 2. Counting the number of interacting and non-interacting densities for the [001] orientation, one finds that there are three densities of each type. The fraction κ of interactions to be removed from Eqs. (19) and (22) must then become 2κ. For the $[\bar{1}11]$ orientation, the same count yields two non-interacting densities for one interacting density; hence κ has to be replaced by $3\kappa/2$. From Eq. (22), the ratio of strain hardening with and without multijunctions, respectively θ_{II} and θ_{II}^{-}, is given by:

$$\left(\frac{\theta_{II}}{\theta_{II}^{-}}\right)_{001} = \frac{1-\kappa/3}{1-2\kappa/3} = 1.125;$$
$$\left(\frac{\theta_{II}}{\theta_{II}^{-}}\right)_{\bar{1}11} = \frac{1-\kappa/2}{1-3\kappa/4} = 1.15 \qquad \text{(C.1)}$$

Thus, omitting multijunctions decreases strain hardening by 12–15%, in agreement with a rule of thumb calculation given in Ref. [29]. In summary, treating junctions as point obstacles significantly increases strain hardening and reduces its orientation dependence, whereas omitting multijunctions reduces strain hardening almost uniformly and by a smaller extent on the [001] and $[\bar{1}11]$ orientations.

References

[1] Gil Sevillano J. Flow stress and work hardening. In: Mughrabi H, editor. Plastic deformation and fracture of materials. Weinheim: VCH; 1993. p. 19.
[2] Nabarro FRN. In: McQueen HJ et al., editors. Strength of metals and alloys, Vol. 3. Oxford: Pergamon Press; 1986. p. 1667.
[3] Mitchell TE. Prog Appl Mater Res 1964;6:117.
[4] Devincre B, Hoc T, Kubin L. Science 2008;320:1745.
[5] Kocks UF, Mecking H. Prog Mater Sci 2003;48:171.
[6] Teodosiu C, Raphanel JL, Tabourot T. In: Teodosiu C, Rapahanel JL, Sidoroff F, editors. Large plastic deformations. Rotterdam: Balkema; 1993. p. 153.
[7] Franciosi P, Berveiller M, Zaoui A. Acta Metall 1980;28:273.
[8] Asaro RJ, Rice JR. J Mech Phys Solids 1977;25:309.
[9] Peirce D, Asaro RJ, Needleman A. Acta Metall 1983;31:1951.
[10] Hoc T, Rey C, Raphanel JL. Acta Mater 2001;49:1835.
[11] Zikry MA, Kao MJ. Mech Phys Solids 1996;44:1765.
[12] Peeters B et al. Acta Mater 2001;49:1607.
[13] Arsenlis A, Parks DM, Becker R, Bulatov VV. J Mech Phys Solids 2004;52:1213.
[14] Cheong KS, Busso EP. J Mech Phys Solids 2006;54:671.
[15] Ma A, Roters F, Raabe D. Acta Mater 2006;54:2169.
[16] Devincre B, Kubin LP, Lemarchand C, Madec R. Mater Sci Eng A 2001;309–310:211.
[17] Madec R, Devincre B, Kubin L, Hoc T, Rodney D. Science 2003;301:1879.
[18] Saada G. Acta Metal 1960;8:841.
[19] Schoeck G, Frydman R. Phys Stat Sol (b) 1972;53:661.
[20] Madec R, Devincre B, Kubin LP. Phys Rev Lett 2002;89(25):255508.
[21] Devincre B, Kubin L, Hoc T. Scripta Mater 2006;54:741.
[22] Devincre B, Kubin L, Hoc T. Scripta Mater 2007;57:207.
[23] Basinski SJ, Basinski ZS. In: Nabarro FRN, editor. Dislocations in solids, Vol. 4. Amsterdam: North-Holland; 1979. p. 261.
[24] Hirth J, Lothe J. Theory of dislocations. Malabar, FL: Krieger; 1992.
[25] Foreman AJE. Philos Mag 1967;15:1011.
[26] Gómez-García D, Devincre B, Kubin LP. Phys Rev Lett 2006;96(12):125503.
[27] Bulatov VV et al. Nature 2006;440:1174.
[28] Madec R, Kubin L. Scripta Mater 2008;56:767.
[29] Takeuchi T. Trans JIM 1975;16:629.
[30] Hoc T, Devincre B, Kubin LP. In: Gundlach C et al., editors. Evolution of microstructures in 3D. Roskilde: Risoe National Laboratory; 2004. p. 43.
[31] Kubin L, Devincre B, Hoc T. Mat Sci Eng A 2008;483–484:19.
[32] Vorbrugg W, Goetting HC, Schwink C. Phys Stat Sol (b) 1971;46:257.
[33] Takeuchi T. J Phys Soc Jpn 1976;40:741.
[34] Schmid H, Kirchner HOK. Philos Mag A 1988;58:905.
[35] Mughrabi H. Mat Sci Eng A 2001;309–310:237.
[36] Jackson PJ. Scripta Mater 1968;2:411.
[37] Carmen Miguel M et al. Nature 2001;410:667.
[38] Zaiser M. Adv Phys 2005;55:185.